PAPER

Check for updates

Growth and properties of ZnO nanorods by RF-sputtering for detection of toxic gases†

Camilla Baratto ID

There is a strong demand for nanostructured materials prepared by an industrially-scalable technique. The current work is devoted to the preparation of ZnO polycrystalline nanorods using RF sputtering at 400 °C and Sn droplets as a catalyzer layer, for highly sensitive gas sensors. Nanorods with diameters ranging from 100 to 200 nm can be tailored by changing the RF power and the deposition time. Raman and PL spectroscopy indicate that the material obtained is ZnO, with a characteristic emission spectrum in the UV region and in the visible. The functional properties of the ZnO nanorods were investigated by studying the response to CBRN (acetonitrile and DMMP), explosive (H_2), and pollutant gases (H_2S, acetone, and NO_2) in the temperature range 200–500 °C. The sensors showed good response to reducing gases at higher temperatures (500 °C) and to NO_2 at lower temperature (200 °C).

A Introduction

Nanoscale semiconductors with controlled morphology and structure are thoroughly investigated due to their promising potential applications in the fabrication of novel functional devices. Among nanostructured materials, one dimensional (1D) metal oxides have received enormous attention due to their high surface to volume ratio, that can be exploited to enhance surface reactions and gas adsorption.

ZnO is a wide band gap semiconductor (E_g = 3.37 eV), with high exciton binging energy (60 meV), that shows interesting optical properties at room temperature.[1,2] ZnO has been investigated for applications in light emitting diodes (LED),[3–5] dye sensitized solar cells,[6] biosensors,[7] and piezoelectric nanogenerators.[8]

For gas sensing application, ZnO is one of the most interesting oxide that was used both for conductometric and optical transduction sensors.[9,10] Detection principle is based on the interaction of gas molecules with ionized oxygen species of O^-, O^{2-} that are on the surface of ZnO in ambient air at a temperature in the range 250–500 °C. The reaction of a reducing gases with the ionized oxygen, releases an electron into the conduction band of ZnO, thus increasing carrier number. For conductometric sensors, the variation is observed by reading an increase in the current.[11]

ZnO 1D materials are usually synthesized as single crystalline nanowires by vapour phase growth technique[12] and hydrothermal growth,[13] while they are prepared as polycrystalline nanorods by plasma enhanced chemical vapour deposition (PECVD),[14] electrochemical anodization[15] and RF-sputtering.[16–18]

Among the cited techniques, sputtering deposition is a well-known, cost effective technology that can be used in large scale plants. Despite this, there are in literature few works that deal with ZnO nanorods prepared by sputtering: ZnO nanorods were grown at low temperature starting from rough Cu layer,[16] Ga doped ZnO buffer layer,[17] of FTO (Fluorine Tin Oxide) thin film.[18] We recently demonstrated that ZnO nanorods were obtained by RF sputtering on magnetic Co/Sn layer:[19] in this case the use of relatively low temperature during growth, allowed to maintain the magnetic properties of the Co layer.

To date, no extensive investigation is present on the growth of ZnO nanorods using a Sn catalyzer. The current paper aims to investigate the growth parameters of ZnO nanorods with Sn catalyzer on an insulating substrate (alumina), and to correlate the physical and morphological properties of the material with its functional properties. Among different gases that can be detected by ZnO gas sensor,[20–22] the current work focuses on dangerous or poisonous gases: H_2 is an explosive gas produced in industrial reactions, Dimethyl Methyl Phosphonate (DMMP) is a simulant of sarin nerve agent (concentration around ppm), NO_2 is an air-pollutant, H_2S is toxic and bad tolerated due to rotten-egg smell, acetonitrile is a simulant for hydrogen cyanide compounds.

B Experimental

Nanorods preparation by RF sputtering

ZnO nanorods were deposited by RF magnetron sputtering system onto 3×3 mm^2 Al_2O_3 substrates. A seed layer of Sn was deposited from Sn target, maintaining the substrate at 400 °C:

CNR-INO & University of Brescia, Sensor Lab, Via Branze 45, Brescia, Italy. E-mail: camilla.baratto@ino.it

† Electronic supplementary information (ESI) available. See DOI: 10.1039/c8ra05357j

Table 1 Samples name and deposition conditions. Ar pressure during deposition was 10^{-2} mbar for all sensors

Sample name	Deposition power (W)	Deposition time (min)
ZNOS10	100	10
ZNOS11	100	15
ZNOS12	150	10
ZNOS13	150	15

since the temperature is higher than Sn melting point, it grows as droplets on the alumina substrate. The droplets act as the catalyst for the subsequent growth of the ZnO nanorods. High pressure deposition (10^{-2} mbar) induced columnar growth resulting into ZnO nanorods. The RF power was varied from 100 to 150 W, while the deposition time was varied from 10 to 15 minutes, as resumed for clarity in Table 1 along with samples' names. The conformation of the obtained layer was very porous due to nanorods formation. The thickness was not measurable with conventional method like profilometer, yet a thicker layer of rods is expected for longer deposition times.

For functional tests with gases, Pt interdigitated electrodes and heater were deposited by RF magnetron sputtering. A Pt meander was deposited on the back-side of the substrate to provide heating by Joule effect. Before the tests, the sensing layers were aged on the TO-5 case by heating the sensors at 500 °C in ambient air for two weeks.

Electron microscopy characterization

The samples' morphology was investigated by scanning electron microscopy (SEM, Zeiss LEO 1525) in conventional mode (recording the secondary electrons with an InLens detector) with an accelerating voltage of 10 kV.

Raman and photoluminescence spectroscopy

Photoluminescence (PL) and Raman spectra were collected using a modular micro-Raman confocal system from Horiba, equipped with a single monochromator and a Peltier-cooled charge-coupled device camera. A solid state laser at 325 nm (PL)/442 nm (Raman) wavelength was used as the excitation source, along with interference filters on the laser lines and edge filters on the signal. For Raman spectroscopy, a $100\times$ objective and 1800 l mm^{-1} grating were used. For PL spectroscopy, a $40\times$ UV objective and 600 l mm^{-1} grating were used.

Functional characterization

Sensing tests were performed in a stainless steel test chamber (1000 cm^3) at an ambient temperature of 20 °C, at atmospheric pressure, using a constant flux (300 cm^3 min^{-1}) with 30% relative humidity (RH). Gas species (acetone, DMMP, acetonitrile, H_2, H_2S, NO_2) were diluted in dry air and contained in certified bottles. A constant bias (1 V direct-current) was applied to the sensing film and the electrical current was measured by a picoammeter (Keithley model 486).

Sensor were tested at constant temperature [300 °C–400 °C–500 °C]. Relative response towards reducing gases (sensor response, R) was calculated as $R = (I_F - I_0)/I_0$, where I_F is the steady state current in gas and I_0 is the steady state current in air. Relative response towards oxidizing gases was calculated as $R = (I_0 - I_F)/I_0$. Response (recovery) times were calculated as the time needed to reach 90% (70%) steady state value in gas (air). Due to the physical constraint of the test chamber (flow 300 cm^3 min^{-1} – and volume 1000 cm^3) a complete exchange of the chamber atmosphere takes more than three minutes, so shorter response and recovery times cannot be evaluated in the present setup.

C Results and discussion

The morphology of the as-grown ZnO layer was characterized by SEM. Since the previous literature on ZnO nanorods showed that there is growth at room temperature from porous copper layer,[17] Cu catalyzer deposited by sputtering was firstly tested; because of low porosity of Cu layer, no directional growth of ZnO was observed – Fig. 1(a).

Growth from FTO thin film at temperatures higher than 400 °C was reported in ref. 16 the authors postulated that the locally presence of SnO on FTO surface decomposed at the deposition temperature (400 °C) and the decomposed metallic Sn reacts with the sputtered Zn to form the liquid phase. The liquid droplets formed on FTO surface act as nucleation sites for ZnO nanorods during sputtering. Taking inspiration from the mechanism involving the liquid phase between Sn and ZnO at temperatures higher than 370 °C (Sn melting point), in the present work we used Sn as the starting seed.

The procedure followed was similar to that used to prepare SnO$_2$ thin films sensors by RGTO (Reothaxial Growth and Thermal Oxidation) technique: in that case a Sn layer is deposited at 400 °C for about 2 minutes, resulting in droplet growth because substrate temperature is higher than 370 °C,[23] followed by oxidation in oven. For ZnO nanorods formation, the need of much smaller tin droplets than those used for SnO$_2$ RGTO thin films, suggested to use very short deposition time (5 s). We experimentally determined that increasing the deposition time of Sn to 10 s and 15 s Sn resulted in the growth of a continuous ZnO film without nanorods development (not shown). Fig. 1(b) shows early growth stages of the sample deposited at 100 W. The alumina substrate is covered by spherical agglomerates with dimension ranging around 50 nm; in some regions tapered nanorods are observable. The nanorods growth direction is randomized with respect to the vertical to the substrate.

As shown in Fig. 1(c) the thinnest rods were obtained by the lowest RF sputtering power (100 W) and 10 minutes deposition (Fig. 1(c)). In this case the diameter of the rod is around 80–100 nm as can be observed in the inset at higher magnification. Some rods are tapered towards the tip to a smaller diameter. Several rods have the longer axes tilted with respect to the normal to the substrate.

The diameter of the rod increased to 150 nm by increasing the deposition time to 15 minutes (Fig. 1(e)). When the deposition power increase to 150 W, the rod diameter increases to 140 nm for 10 minutes deposition – Fig. 1(d) – and 190 nm for
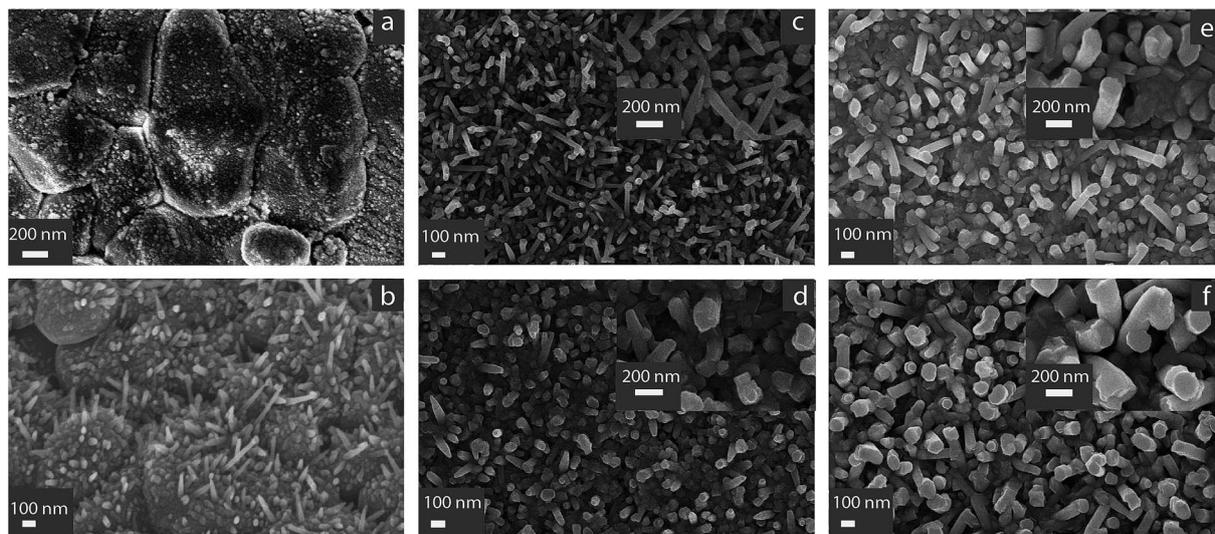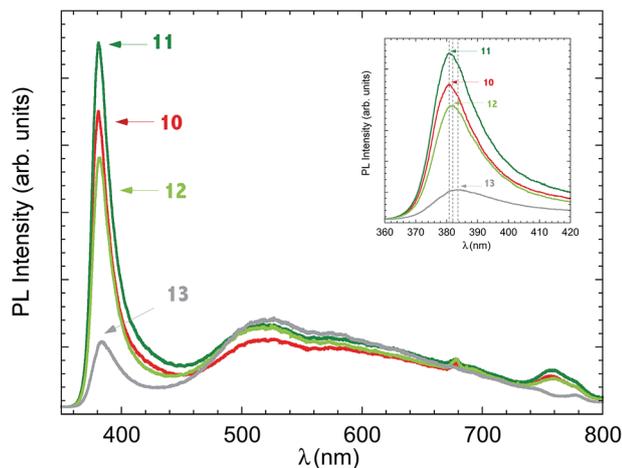
Fig. 3 PL spectra of ZnO nanorods sensors acquired at room temperature. The ratio of the NBE emission over defect emission is considered a measure of the crystalline quality of the ZnO. (Inset) Detail of NBE emission: a blue shift in the peak position can be observed going from sample ZNOS13 to ZNOS10. Dotted lines are merely a guide for the eye.

Gas sensing tests

The gas sensing tests were carried out to test the performances of ZnO nanorods as gas sensors and to test the influence of sample morphology on the sensing properties. The working temperature was varied from 200–500 °C by a 100 °C steps.

Fig. 4 shows response to NO_2 (1–1.5–2 ppm) for the best performing sensor ZnOS12. NO_2 behave as an oxidizing gas, inducing a decrease in the current when the temperature ranged from 200 °C to 400 °C. The noise observed at 400 °C is due to a disturbance during the measurements. Response and recovery times at 200 and 300 °C are of the order of minutes,
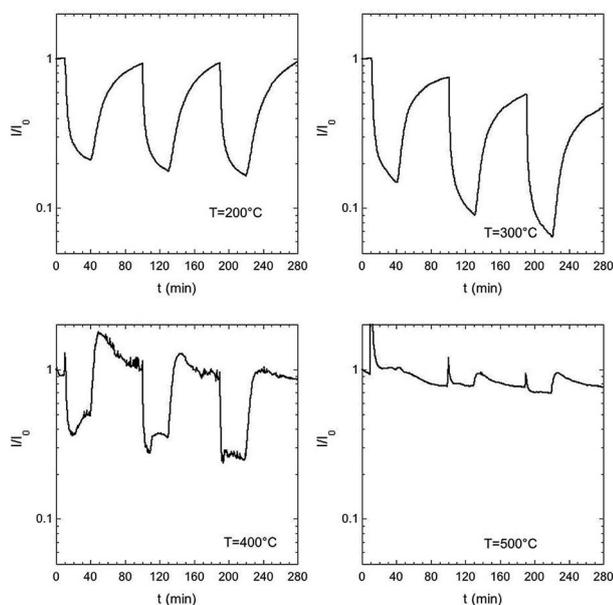

Fig. 4 Dynamic curves for sensor ZNOS12 when NO_2 (1–1.5–2 ppm) was introduced. Gas carried wad humid air (30%) at room temperature.
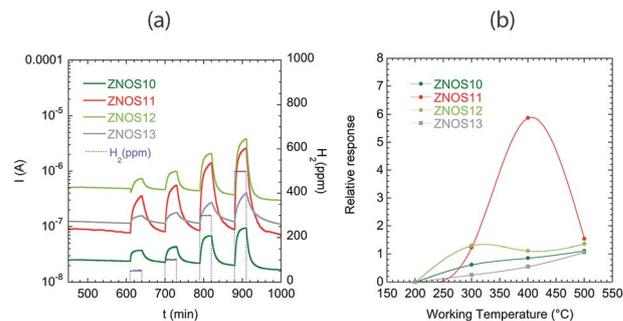

Fig. 5 (a) Dynamic curve of the tested sensors at 400 °C towards 50–100–200 and 300 ppm of H_2; (b) relative response to 100 ppm of H_2 at different temperatures for all sensors; the lines between experimental point are a guide for the eyes.

while they decrease at 400 °C at the expense of sensor response. At 500 °C no detection of NO_2 was observed.

Hydrogen is an explosive gas, thus detection at concentration much below the Lower Explosion Limit (LEL, equal to 4%) is very important. The range of concentrations analysed here was [50–300 ppm]. Fig. 5(a) shows the sensing behaviour of the ZnO sensors towards H_2 at 400°C: the analysis of the dynamic current variation, demonstrated a complete recovery of the baseline. ZnOS11 was the best performing sensor. ZNOS11 and ZNOS13 showed increased response and recovery times with respect to ZNOS11 and ZNOS12. Referring to SEM image (Fig. 1), we can observe that the slower sensors are the one with bigger nanorods – Fig. 1(e) and (f).

Fig. 5(b) reports the sensing behaviour of all sensors with H_2 in the analysed temperature range. ZnO based sensors showed good relative responses to H_2 at 400 and 500 °C. At 300 °C a detection was evident, but the sensor dynamic was too slow (not shown).

Fig. 6(a–d) shows relative responses of the tested sensors to low concentrations of H_2S (3–5–7 ppm) from 300 °C to 500 °C. H_2S behave as a reducing gas: an increase in sensor current was observed for ZnO based sensors. ZnO nanorods were sensible to H_2S presence even at 300 °C but the relative response washigher at 500 °C. Response and recovery times decreased from 300 °C to 500 °C, being of the order few minutes at 500 °C.

The better sensors for H_2S are ZNOS10 and ZNOS12, working at 500 °C; the data in Fig. 6(a) and (c) were fitted by a power law response $= A \times [\text{concentration}]^B$. Extrapolation of data fit to axis limit (ESI, see Fig. S1†) showed that the limit of detection for ZNOS10 is 0.1 ppm, while for ZNOS12 is 0.2 ppm.

At 500 °C the dynamic curves for the two sensors were comparable – Fig. 6(e) – while the worse response was observed for ZnOS11. ZNOS11 and ZNOS13 showed also slower recovery of the baseline value: these sensors were the ones with bigger rods diameter.

ZnO nanorods prepared by RF sputtering have performances much better compared to those obtained with ZnO single crystalline nanowires,[30] being $\Delta R/R = 0.25$ to 5 ppm for sensor analyzed in the reference, while in our case $\Delta R/R = 200$ to the same concentration for ZNOS10 sensor.
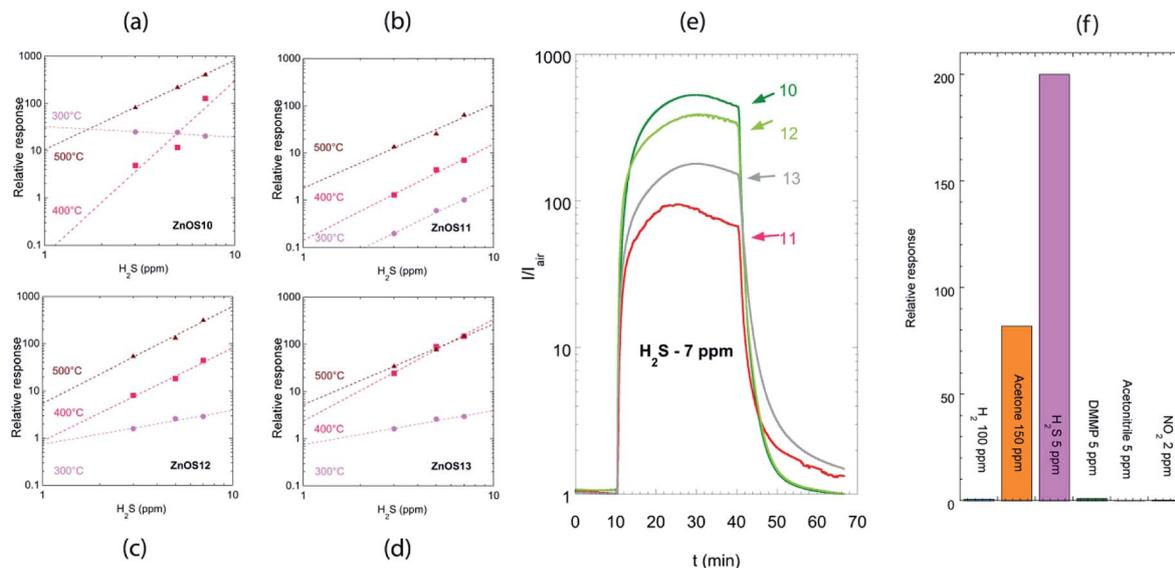
Fig. 6 Relative response to 3–5–7 ppm of H_2S in the temperature range [300 °C–500 °C] for (a) ZNOS10, (b) ZNOS11, (c) ZNOS12, (d) ZNOS13; the dotted line are the fit of the data with a power law. (e) Dynamic curve of sensors at 500 °C towards 7 ppm of H_2S. (f) Selectivity to 6 gases measured for ZnOS10 sensor at 500 °C.

There is debate in literature on the mechanism responsible for H_2S detection with ZnO. Chen et al.[31] claimed that the high sensing capabilities of 20–50 nm diameter ZnO nanowires to ppm level H_2S was due to sulfuration reaction when H_2S was introduced into test chamber. Instead, the reaction scheme usually associated with the detection of reducing gases in metal oxide semiconductors, takes into account the reaction of H_2S with oxygen ionosorbed over the surface, with a consequent release of electrons into the conduction band.[32] In the present work, the latter mechanism is more probable due to higher dimension of the nanorods used, and to the higher working temperature used. Moreover, in the conventional sensing mechanism, the calibration curve was described by a power law, while in the case of sulfuration reaction the calibration curve was fitted with a line.[31]

Fig. 6(f) shows the comparison of the sensor response towards six different species: five reducing gases (H_2, acetone, H_2S, DMMP and acetonitrile), and one oxidizing gas (NO_2). At 500 °C, response to H_2S is two orders of magnitude higher than response to H_2 and DMMP (0.8 and 1 respectively), and three orders of magnitude higher than response to NO_2 and to acetonitrile (0.3 and 0.2 respectively). The response is only one order of magnitude higher than the response to acetone, for which indeed the concentration is much higher (150 ppm versus 5 ppm).

We can thus observe partial selectivity towards H_2S at 500 °C. At lower temperatures (200 °C), no response to reducing gases is observed, thus the sensors are partially selective to NO_2 in this temperature range. A feasible approach to lower the cross-sensitivity of ZnO material in view of the sensor application, is the use of one ZnO sensor working at 500 °C and another ZnO sensor working at 200 °C in an array configuration: higher selectivity can be gained using pattern recognition.[33]

D   Conclusions

In summary, ZnO polycrystalline nanorods was easily prepared by RF sputtering, starting from Sn catalyzer. The diameter of ZnO nanorods was controlled by changing the deposition power and the growth time. The rod diameter ranges from 100 nm to 150 nm for 100 W power and from 140 nm to 190 nm for 150 W power.

PL and Raman spectroscopies showed that the material obtained is ZnO with the typical emission spectrum in the UV region and in the visible. The quality of UV emission is higher for samples deposited at lower power.

The analysis of the gas sensing properties of the ZnO nanorods showed that they are very promising for detection of CBRN (acetonitrile and DMMP), explosive (H_2), and pollutant gases (H_2S), with some selectivity towards H_2S at high temperature. Selectivity to NO_2 detection can be obtained working at lower temperatures (200 °C). A smaller diameter of the nanorods is in general useful to achieve better sensor response. The results obtained are highly relevant in view of the strong demand for nanostructured materials prepared using an industrially-scalable technique.

Conflicts of interest

There are no conflicts to declare.

Acknowledgements

References

1 J. M. Bao, M. A. Zimmler, F. Capasso, X. W. Wang and Z. F. Ren, *Nano Lett.*, 2006, **6**, 1719–1722.

2 M. H. Huang, S. Mao, H. Feick, H. Q. Yan, Y. Y. Wu, H. Kind, E. Weber, R. Russo and P. D. Yang, *Science*, 2001, **292**, 1897–1899.

3 S. Xu, C. Xu, Y. Liu, Y. F. Hu, R. S. Yang, Q. Yang, J. H. Ryou, H. J. Kim, Z. Lochner, S. Choi, R. Dupuis and Z. L. Wang, *Adv. Mater.*, 2010, **22**, 4749–4753.

4 X. M. Zhang, M. Y. Lu, Y. Zhang, L. J. Chen and Z. L. Wang, *Adv. Mater.*, 2009, **21**, 2767–2770.

5 C. Baratto, R. Kumar, E. Comini, G. Faglia and G. Sberveglieri, *Opt. Express*, 2015, **23**, 18937–18942.

6 O. Lupan, V. M. Guerin, I. M. Tiginyanu, V. V. Ursaki, L. Chow, H. Heinrich and T. Pauporte, *J. Photochem. Photobiol., A*, 2010, **211**, 65–73.

7 D. Pradhan, F. Niroui and K. T. Leung, *ACS Appl. Mater. Interfaces*, 2010, **2**, 2409–2412.

8 J. W. Zhong, Q. Z. Zhong, F. R. Fan, Y. Zhang, S. H. Wang, B. Hu, Z. L. Wang and J. Zhou, *Nano Energy*, 2013, **2**, 491–497.

9 O. Lupan, L. Chow, T. Pauporte, L. K. Ono, B. R. Cuenya and G. Chai, *Sens. Actuators, B*, 2012, **173**, 772–780.

10 C. Baratto, S. Todros, G. Faglia, E. Comini, G. Sberveglieri, S. Lettieri, L. Santamaria and P. Maddalena, *Sens. Actuators, B*, 2009, **140**, 461–466.

11 N. Barsan, M. Schweizer-Berberich and W. Gopel, *Fresenius' J. Anal. Chem.*, 1999, **365**, 287–304.

12 Z. M. Zhu, T. L. Chen, Y. Gu, J. Warren and R. M. Osgood, *Chem. Mater.*, 2005, **17**, 4227–4234.

13 L. Vayssieres, *Adv. Mater.*, 2003, **15**, 464–466.

14 X. Liu, X. H. Wu, H. Cao and R. P. H. Chang, *J. Appl. Phys.*, 2004, **95**, 3141–3147.

15 V. Galstyan, E. Comini, C. Baratto, A. Ponzoni, E. Bontempi, M. Brisotto, G. Faglia and G. Sberveglieri, *CrystEngComm*, 2013, **15**, 2881–2887.

16 M. Yang, H. C. Kim and S. H. Hong, *Thin Solid Films*, 2014, **573**, 79–83.

17 M. T. Chen and J. M. Ting, *Thin Solid Films*, 2006, **494**, 250–254.

18 S. W. Kan, S. K. Mohanta, Y. Y. Kim and H. K. Cho, *Cryst. Growth Des.*, 2008, **8**, 1458–1460.

19 R. Ciprian, C. Baratto, A. Giglia, K. Koshmak, G. Vinai, M. Donarelli, M. Ferroni, M. Campanini, E. Comini, A. Ponzoni and G. Sberveglieri, *RSC Adv.*, 2016, **6**, 42517–42521.

20 E. Comini, C. Baratto, G. Faglia, M. Ferroni, A. Vomiero and G. Sberveglieri, *Prog. Mater. Sci.*, 2009, **54**, 1–67.

21 S. Morandi, A. Fioravanti, G. Cerrato, S. Lettieri, M. Sacerdoti and M. C. Carotta, *Sens. Actuators, B*, 2017, **249**, 581–589.

22 M. Tonezzer, T. T. L. Dang, N. Bazzanella, V. H. Nguyen and S. Iannotta, *Sens. Actuators, B*, 2015, **220**, 1152–1160.

23 G. Sberveglieri, *Sens. Actuators, B*, 1992, **6**, 239–247.

24 V. Russo, M. Ghidelli, P. Gondoni, C. S. Casari and A. L. Bassi, *J. Appl. Phys.*, 2014, **115**, 073508.

25 K. Vanheusden, W. L. Warren, C. H. Seager, D. R. Tallant, J. A. Voigt and B. E. Gnade, *J. Appl. Phys.*, 1996, **79**, 7983–7990.

26 J. Q. Hu and Y. Bando, *Appl. Phys. Lett.*, 2003, **82**, 1401–1403.

27 B. X. Lin, Z. X. Fu and Y. B. Jia, *Appl. Phys. Lett.*, 2001, **79**, 943–945.

28 Y. H. Yang, X. Y. Chen, Y. Feng and G. W. Yang, *Nano Lett.*, 2007, **7**, 3879–3883.

29 S. A. Studenikin and M. Cocivera, *J. Appl. Phys.*, 2002, **91**, 5060–5065.

30 H. Y. Huang, P. C. Xu, D. Zheng, C. Z. Chen and X. X. Li, *J. Mater. Chem. A*, 2015, **3**, 6330–6339.

31 Y. Chen, P. C. Xu, T. Xu, D. Zheng and X. X. Li, *Sens. Actuators, B*, 2017, **240**, 264–272.

32 K. D. Diao, M. J. Zhou, J. C. Zhang, Y. J. Tang, S. X. Wang and X. D. Cui, *Sens. Actuators, B*, 2015, **219**, 30–37.

33 X. Liu, S. Cheng, H. Liu, S. Hu, D. Zhang and H. Nin, *Sensors*, 2012, **12**, 9635–9665.